JOURNAL OF OPTOELECTRONICS AND ADVANCED MATERIALS Vol. 9, No. 4, April 2007, p. 799 - 809

Invited Paper

Molecular dynamics simulation of defect formation in irradiated face centered cubic materials

D. ŞOPU, D. M. POPOVICI[a], M. A. GÎRŢU[*]
Department of Physics, Ovidius University of Constanţa, Constanţa, 900527, Romania
[a]Department of Mathematics and Computer Science, Ovidius University of Constanţa, Constanţa, 900527, Romania

There are presented molecular dynamics simulations of collision cascades in various metals (Al, Cu, Ni, Pb) irradiated with ions of up to 1000 eV kinetic energy, with the aim of studying the degradation of the physical properties of some face centered cubic metallic materials used in nuclear power plants. We simulated systems of up to 37000 atoms using periodic boundary conditions only along the transverse directions, perpendicular to the direction of the initial impact. We kept the system at constant temperature, and performed multiple runs, changing slightly and randomly the direction of the projectile ion. We studied the time evolution of the defects induced by irradiation and we analyzed various numbers of multiple vacancies (mono-, di-, tri-, and tetra- vacancies). We find that, for all materials, although during the collision cascade, due to local melting, some regions of the sample become amorphous, during the relaxation phase the atoms tend to return to their equilibrium positions and the systems recrystallize. The smallest number of defects and the fastest recrystallization was observed in the case of Ni. The largest path through the target and number of defects was seen for Al, while the slowest lattice relaxation regeneration was found for Pb.

(Received November 2, 2006; accepted February 28, 2007)

Keywords: Ion irradiation, Collision cascades, Thermal spike, Local melting, Frenkel defects, Recrystallization, fcc metals

1. Introduction

The study of the irradiation-induced defect formation in various metals and metal alloys is of interest in order to understand the degradation of the physical properties of the materials used in pressure vessels in nuclear power plants as well as in metal coatings for fusion-based alternative energy sources [1]. The theoretical description of radiation effects in materials requires modeling and simulation of processes that occur over widely disparate length and time scales [2,3]. Since most damage produced in materials during ion irradiation derives from a complex process occurring in collision cascades, much research has been devoted to studying these events [4]. While collision cascades produce defects in a region of the order of nanometers and on a time scale of tens of picoseconds, being easily modeled by molecular dynamics, defect migration and diffusion occurs over longer time scales, of the order of nanoseconds and milliseconds, or larger, respectively, and can be simulated by kinetic Monte Carlo; even further, the changes in the microstructure can be studied by finite element methods or discrete dislocation dynamics and imply time scales of the order of seconds or larger [2,3].

Molecular dynamics (MD), by virtue of its simplicity and the appropriateness of the time and length scale, is an extremely powerful tool to obtain atomic-scale information and physical insight into the mechanisms of radiation-induced defect production [1,2]. MD simulations have been used extensively in the past for the purpose of modeling defect production for recoils starting at the beginning in the range 0.1 to 50 keV [2] and continuing, more recently, with energies of 50 to 200 keV [4].

Recoil-induced cascades of energetic atomic displacements give rise to a highly non-equilibrium concentration of point defects and point defect clusters [2,5]. Over macroscopic length and time scales these defects can migrate, often inducing significant degradation of mechanical and other properties [1]. Irradiation of materials by high-energy ions produces Frenkel pairs [6], which are interstitial-vacancy pairs. The migration of these individual defects leads to either their recombination or to the formation of vacancy or interstitial clusters [1]. While in semiconductors amorphous clusters are produced in the cascade core, in metals most of the crystal regenerates, leaving only small vacancy-rich clusters [7]. Moreover, recently, a study of the defect kinetics in irradiated iron showed that the barriers to migration of multiple vacancies are low, suggesting that the vacancies can move through the solid in clusters of various sizes [6].

In this article we study the production of Frenkel pair defects during the collision cascades produced by a recoil atom with the initial kinetic energy of up to 1000 eV in a target of up to 37000 atoms. We study the time evolution of the resulting vacancies as well as their migration towards the surface. We choose for our study fcc materials that are commonly used in pressure vessels in nuclear power plants, Al, Cu, Ni, and Pb, ranging from light to heavy metals. For all systems we find that the closed packed structure plays an important role in the fast regeneration of the crystal after the collision cascade.

2. Model and principles of the simulation

In molecular dynamic simulations the time evolution of a system of atoms is determined by solving the equations of motion numerically [8,9]. In the Newtonian formalism the force acting on an atom is calculated based on the sum of the contributions of all other particles, taking into account the gradient of the interatomic potential [8].

We employed in the simulation the Morse pair potential [10], selected both for its simplicity, and for allowing a good fit to the real interparticle potential for many simple metals with a fcc structure [11]. The expression of the Morse potential is [10]

$$V(r) = D_e e^{-2\alpha(r-r_e)} - 2D_e e^{-\alpha(r-r_e)}, \qquad (1)$$

where r is the distance between the atoms, r_e is the equilibrium distance between the two atoms, D_e is the 'depth' of the potential energy function, and α controls the 'width' of the potential. For the metals of interest here the values of these constants are displayed in Table 1 [11].

Table 1. Values of the parameters used in the Morse potential according to ref. [11].

Metal	r_e (Å)	α (Å^{-1})	D_e (eV)
Al	3.253	1.1646	0.2703
Cu	2.866	1.3588	0.3429
Ni	2.780	1.4199	0.4205
Pb	3.733	1.1836	0.2348

The infinite range of the potential implies that every particle interacts with all the other particles. As the simulated systems grow larger and larger the number of force computations grows with the square of the number of particles, leading to long computer times for each run. A partial solution to this problem is the potential truncation, suggested by the rapid decrease of the strength of the interaction at large distances. A typical cutoff radius for the Morse potential is $r_c = 1.8\, r_e$ [8].

After the force calculation, the equations of motion for the system are solved using an integration algorithm, which provides the new positions and velocities for each particle. The equations of motion for the typical equilibrium simulation, performed at constant temperature, are given simply by Newton's second law. One of the most common integration algorithms is the so called velocity Verlet algorithm [12], whose defining relations are:

$$\mathbf{r}(t+\Delta t) = \mathbf{r}(t) + \mathbf{v}(t)/\Delta t + \mathbf{a}(t)\Delta t^2/2 \qquad (2)$$

$$\mathbf{v}(t+\Delta t) = \mathbf{v}(t) + [\mathbf{a}(t) + \mathbf{a}(t+\Delta t)]\Delta t/2 \qquad (3)$$

The new positions, $\mathbf{r}(t+\Delta t)$, and velocities, $\mathbf{v}(t+\Delta t)$, are determined based on the positions, $\mathbf{r}(t)$, and velocities, $\mathbf{v}(t)$, at the previous moment and the accelerations at both the previous, $\mathbf{a}(t)$, and the present, $\mathbf{a}(t+\Delta t)$, time.

The simulations were performed on a personal computer with an Intel Dual Core processor running at 3.0 GHz clock speed, using an in house program written in C based on the MDRANGE program [13]. The collision cascades and the time evolution of the number of vacancies was examined by simulating up to 20 events, with initial energies of the projectile particle of up to 1000 eV, for simulation times of up to 10 ps. The initial position of the projectile atom was chosen at $2\,r_e$ in front of the target. The initial kinetic energy was distributed mostly on the longitudinal velocity, allowing however a small transverse component, chosen randomly for each of the 20 events, of at most 10% of the longitudinal one.

The initial energy was chosen at 100, 200, 500 and 1000 eV, based on two main competing criteria. First, sufficient energy is needed to cause major collision cascades, relevant to describe the defect generation and the time evolution of the vacancies. Statistical relevance can be obtained if more than only a few vacancies (say 30 such vacancies) are produced in one recoil event [14]. Secondly, the energy had to be small enough to prevent the complete passage through the target. Constraints related to the time and computer power available lead to the choice of a system of up to 37044 atoms (42x42x21 atomic layers). Most simulations were performed for systems of 13500 atoms (30x30x15 atomic layers) and a few for systems of 5324 atoms (22x22x11 atomic layers). The passage through the target can be prevented if the system has 25-40 atoms for each eV of the incoming ion [1].

To simulate a large system we used periodic boundary conditions along the transverse directions, perpendicular to the direction of the initial impact. Along the longitudinal axis the boundaries are free, to better describe the surface phenomena and to prevent the reflection from the border. The target was previously equilibrated at room temperature, 300 K, and atmospheric pressure by scaling the velocities and the positions of all particles, using the Berendsen approach [15] with a time constant of $100\Delta t$. The equilibration times were different for each target size and for each material, ranging from 5000 for Cu to 35000 fs for Pb.

During the simulation, the temperature of the system was brought towards room temperature by scaling the velocities [15]. The pressure, however, was not kept constant, mostly because of the free longitudinal surfaces.

The total number of vacancies was determined counting all the original sites that were empty (for which no atom could be located within half the nearest-neighbor distance). The numbers of the various multiple vacancies (i.e. mono-, -di, -tri, -tetra, vacancies) were calculated by examining for emptiness the nearest neighbors of each vacant site. We note that the total number of vacancies, N_V, expected after ion irradiation can be determined, at the end of the relaxation phase, based on Kinchin-Pease equation [16]:

$$N_v = \frac{E_K}{2E_d} \qquad (4)$$

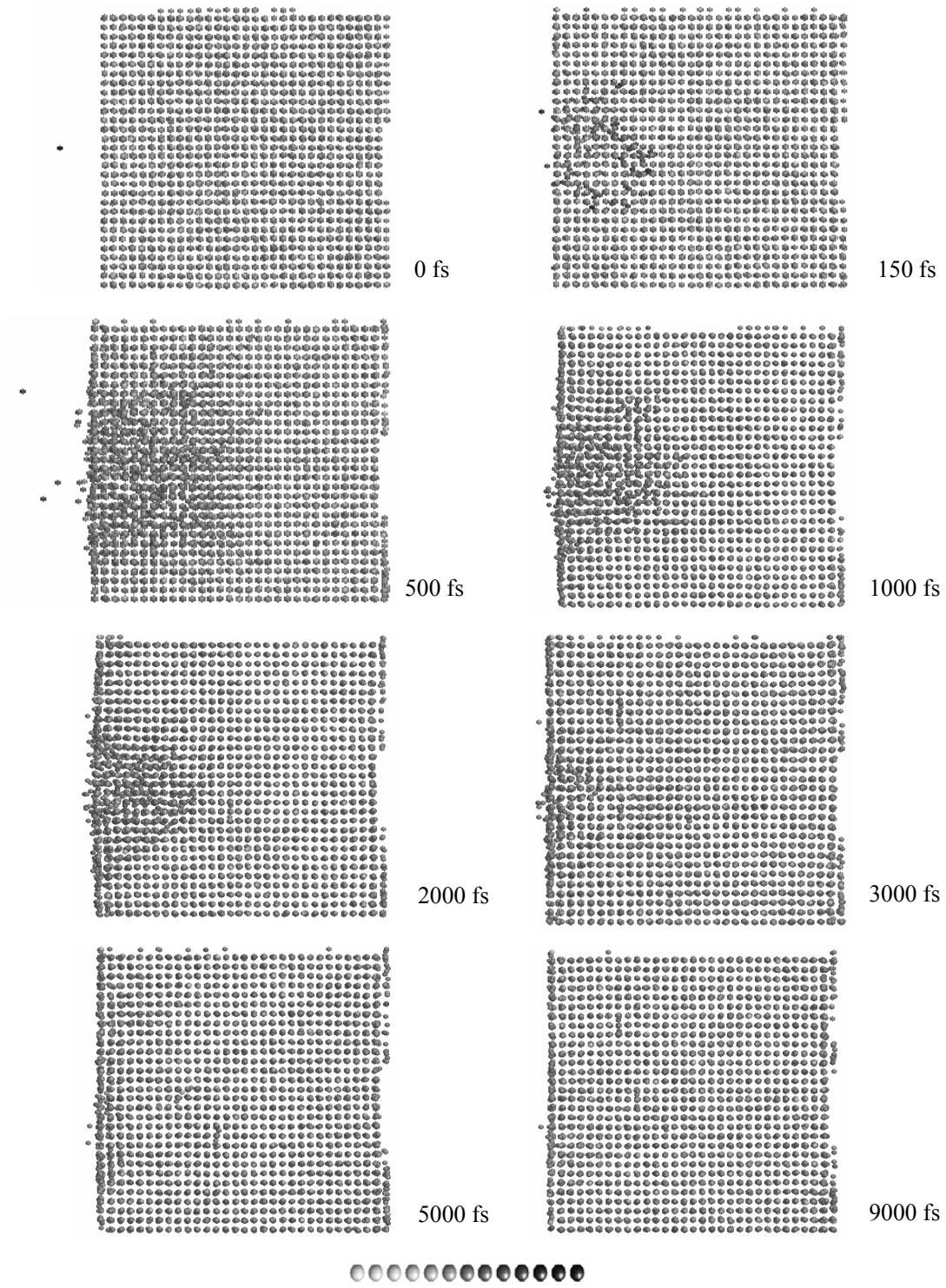

Fig. 1. Lateral view of a 500 eV collision cascade in Cu, at various times, visualized with RasMol. Note that, for clarity, the five particles that escaped from the solid are omitted for $t \geq 1000$ fs. Inset: The grey scale energy coding: from left to right, the kinetic energy is: $E_k < 0.005$ eV, 0.005-0.03 eV, 0.03-0.06 eV, 0.06 - 0.10 eV, 0.10-0.14 eV, 0.14-0.20 eV, 0.20-0.35 eV, 0.35-0.50 eV, 0.5-0.7 eV, 0.7-1.2 eV, 1.2-5 eV, 5-25 eV, > 25 eV.

where E_K is the kinetic energy of the projectile ion and $2E_d$ is the defect formation energy for Frenkel pairs [17]. The values of the parameter E_d have been determined empirically, for cooper being about 40 eV [18]. Thus, eq. (6) predicts that the final number of Frenkel pair defects produced by one 500 eV collision event for copper should be approximately 6.

The positions and kinetic energies of each particle of the system were displayed using the open source software RasMol [19], which allows 3D visualization from various angles. It has the advantage that it can easily display large systems, the color coding (or the grayscale) indicating qualitatively, the kinetic energy of each particle. The disadvantage, however is that it does not allow for different transparencies of various particles to better visualize particular parts of the systems (for instance the hot regions with high energy particles, displaced from their equilibrium positions).

To obtain a more flexible visualization software than RasMol, we implemented our own virtual reality based software, ScientView, [20] based on the ARéVi API developed by CERV [21,22]. ARéVi is an open C++ and OpenGL based source, and is adaptive to very different configurations, starting from desktop systems and ending with 3D stereoscopic immersion systems. ScientView allows the immersion within the simulated virtual environment leading to an interactive 3D visualisation of the experiment. Like RasMol, it allows various visualization perspectives, from different angles, but it also permits the navigation through the simulated environment for instance following the impact particle (or any other particle of the system). Another special feature is the capability to modify the level of transparency of various particles which allows a clearer picture of the shock wave and the molten regions. Moreover, other options are related to sequences of images, the user being able to switch between no animation, step by step and continuous interpolation-based animation modes. The software also allows for reverse display of the time evolution as well as for choosing and visualising particles in any section plane parallel to the walls of the simulating cell.

3. Results and discussion

One of the 500 eV collision cascades events simulated for Cu is shown in Fig. 1. The grayscale coding shown in the inset of Fig. 1, is a logarithmic scale representing the kinetic energy of the particle, with ranges from high energies (dark grey) to room temperature energies (light grey). We note that during the collision, five particles leave the target with enough kinetic energy to never return. To preserve the scale, the area represented is the same at all time steps and, for that reason, the five particles that escaped from the solid are omitted in Fig. 1 for $t \geq 1000$ fs.

The damaging effects of the collision are spectacular, as the energy of the incoming particle is transferred to the target atoms, causing major defect formation (see Fig. 1). It can be seen that, although the projectile follows a downward path, there are secondary recoil particles with upward trajectories, suggesting conservation of momentum in the initial collision stage. The principal recoil shock wave is displayed at 150 fs after the impact. After 500 fs, the atoms in the impact region have moved from their equilibrium positions, indicating the local melting of the target. The melting indicates heat dissipation from the projectile and secondary recoil particles to the solid, suggesting that the collision phase lasts less than 500 fs.

The collision phase is followed by the thermal spike phase, which allows for heat dissipation. From Fig. 1 it can be seen that the thermal spike starts from the main recoil particle and from the secondary recoil particles and propagates through the solid. After 1000 fs the atoms have already released a large part of their energy and have started to relocate. The melted region is about to recrystallize and, therefore, the thermal spike phase ends before 1000 fs.

The relaxation phase starts before 1000 fs and lasts longer than the 10 ps simulated. As time passes the defects migrate from the bulk towards the surface, as shown in Fig. 1. Following the cooling down process taking place during the thermal spike, the amorphous pockets left from the melted regions recrystallize. The recrystallization process starts in the bulk and evolves towards the surface and is not complete, some defects being left behind, as they are unable to migrate.

Moving from the representation of the collision cascade to that of the defects generated in the collision event shown in Fig. 1, we display in Fig. 2 the time evolution of all the vacancies. It can be seen that at the beginning of the collision phase the vacancies are preponderantly produced along the main recoil direction and in a small number on the secondary recoil directions. As time passes, the defects spread in the bulk being produced in clusters (connected vacancies) in the volume of the sample. A large number of vacancies is observed at 1000 fs, a large fraction being distributed at the surface.

After 1000 fs the total number of vacancies decreases. The defects start migrating from the bulk towards the surface and the defect clusters break into smaller clusters, increasing the number of mono-vacancies. Some of the vacancies remain trapped in the bulk even after 3000 fs, surviving even the slow relaxation phase that follows. Our results are in agreement with the description of migration of vacancies and interstitials of Nordlund and Averback [18].

The results of ten individual 500 eV collision events in Cu and their average are shown in Fig. 3. It can be seen that during the first 300 fs the number of vacancies rises almost equally abruptly for all the events but afterwards fluctuations occur. It is interesting that the width of the fluctuation range seems to remain approximately the same over the 10 ps of the simulation. The maximum number of vacancies is reached at about 1000 fs, which confirms the qualitative conclusions drawn from Fig. 2. After 1000 fs, in the relaxation phase, the number of vacancies decreases slowly. After 3 000 fs the total number of vacancies is about 30 and continues to decrease slowly towards the number of vacancies predicted by the Kinchin-Pease

relation (Eqn. 4). Indeed, Fig. 2 shows at 9000 fs a small number of bulk vacancies, most vacancies left being located on or near the surface of impact.

The time evolution of the various average numbers of multiple vacancies is shown in Fig. 4. The numbers of complex (di-, tri-, and tetra-) vacancies increase fast at the beginning of the 500 eV collision cascade in Cu, but decrease slowly after that, whereas the number of mono-vacancies decreases much later. The numbers of multiple vacancies reach maxima at about 1000 fs, and afterwards fluctuate, decreasing slowly. The time evolution of the various types of multiple vacancies indicates that the defect clusters tend to break into smaller pieces during the recrystallization process, consistent with the results of Fig. 2.

A similar analysis was made for Ni, Pb and Al. Because of space limitations we do not present for all these materials all the figures corresponding to those of Cu. We parallel and contrast the four systems, concentrating instead on the major similarities and differences between them.

In the case of Ni, the projectile enters the target without causing significant damage on the surface (see Fig. 5). As the secondary recoils are almost isotropic, the region of atoms displaced due to the impact is roughly spherical and well localized. The recrystallization process is very fast and relatively uniform in the bulk, leading to a small number of defects.

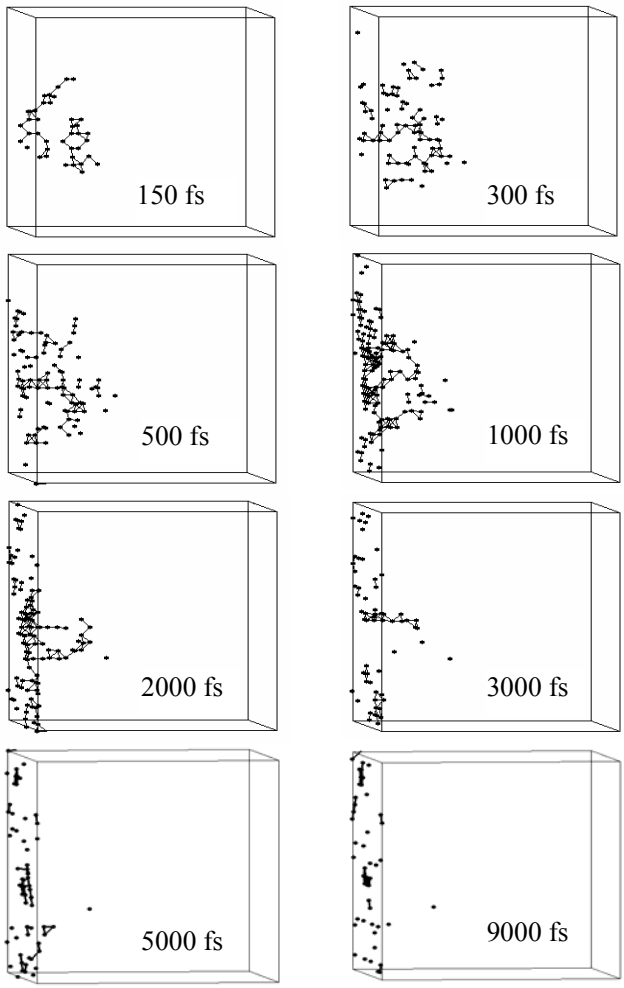

Fig. 2. Time evolution of all vacancies formed in a collision event in Cu, irradiated with a 500 eV ion (from Fig. 1), displayed using RasMol. The vacancies are represented with dots while the vacancy clusters are connected with lines.

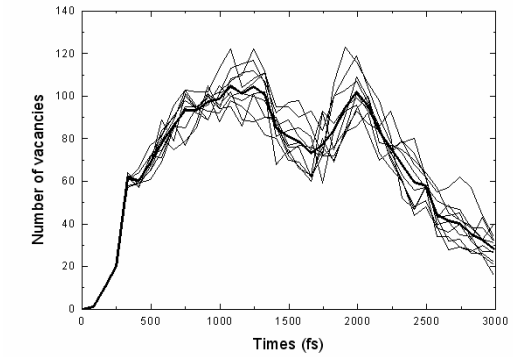

Fig. 3. Time evolution of the total number of vacancies produced in Cu irradiated with a 500 eV ion. Ten individual events (with randomly selected initial recoil direction) and the average (thick line) are shown.

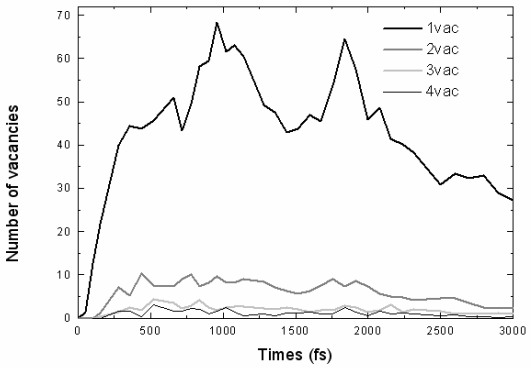

Fig. 4. Time evolution of the number of vacancies of mono-, di-, tri- and tetra-vacancies generated in a Cu target by a 500 eV ion. The lines are averages calculated over 10 collision events.

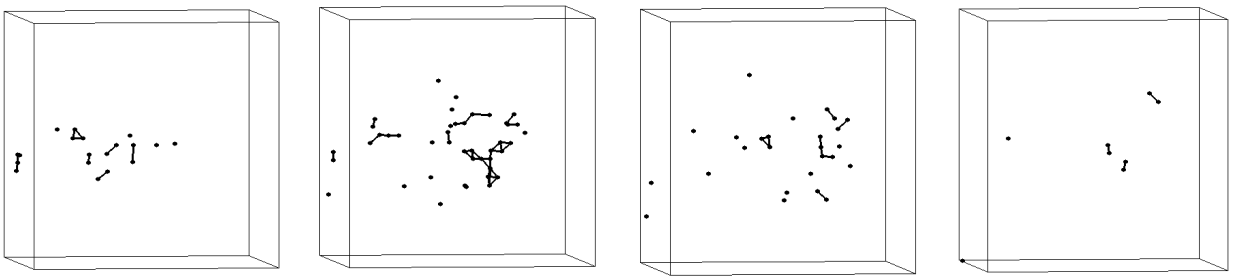

Fig. 5. Time evolution of all vacancies formed in a collision event in Ni, irradiated with a 500 eV ion, displayed using RasMol. The vacancies are represented with dots while the vacancy clusters are connected with lines.

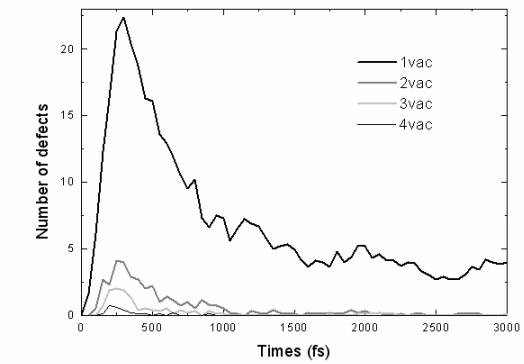

Fig. 6. Time evolution of the number of vacancies of mono-, di-, tri- and tetra-vacancies generated in a Ni target by a 500 eV ion. The lines are averages calculated over 10 collision events.

The multiple defects tend to break apart during the recrystallization as seen in both Fig. 5 and Fig. 6. The peaks in all average numbers of multiple vacancies (for 500 eV collision events) are located before 300 fs and are very sharp with widths of less than 700 fs.

The generation of defects for Pb (Fig. 7) is different form the previous two cases. It resembles the case of Cu in the sense that there are some major directions of recoil (which make the distribution of defects strongly anisotropic) and that the surface defects are numerous. However, unlike Cu but similar to Ni, the clusters of multiple vacancies are less numerous.

The decrease of the number of vacancies is very slow (Fig. 8). Although the maxima are reached at around 1000 fs, after 3000 fs all numbers of multiple vacancies fluctuate strongly, displaying a decrease of at most 10%. The fluctuations of the various numbers of multiple vacancies seen in Fig. 9 can be correlated with the migration of defects towards the surface, observed in Fig. 7.

A more spectacular observation was made when analyzing the case of the impact of a 1000 eV particle on a 37044 atom Pb target. As shown in Fig. 9, at 400 fs the defects are formed both at the surface and along the main recoil direction. As time passes, the shock wave causes more defects on the surface but also secondary recoil in the bulk. After 3000 fs the number of vacancies in the bulk has decreased both due to recrystallization and to migration to the surface. The initial energy is large enough in this case for the projectile to penetrate far enough in the target to allow for a separation between the bulk and surface defects. This effect was not noticeable in the case of a 500 eV ion, presented in Fig. 7.

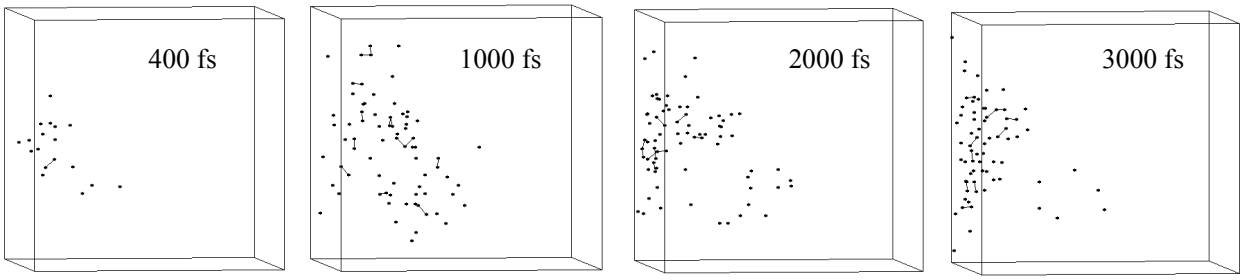

Fig. 7. Time evolution of all vacancies formed in a collision event in Pb, irradiated with a 500 eV ion, displayed using RasMol. The vacancies are represented with dots while the vacancy clusters are connected with lines.

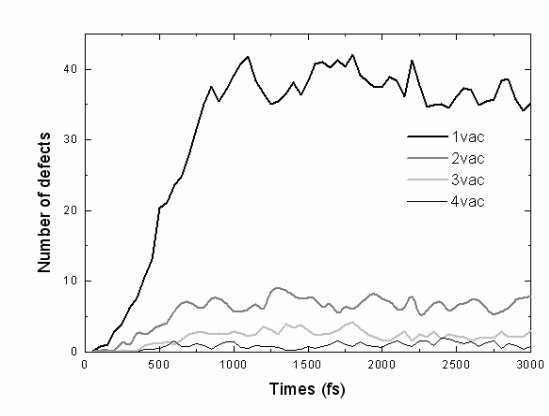

Fig. 8. Time evolution of the number of vacancies of mono-, di-, tri- and tetra-vacancies generated in a Pb target by a 500 eV ion. The lines are averages calculated over 10 collision events.

The ScientView image of the actual system in the case of 1000 eV ion impinging on the 37044 atom target is displayed in Fig. 10. ScientView's capability to control the transparency of the target atoms is remarkably useful. In Fig. 10 it can be seen that when the transparency is zero (the image being similar to the one offered by RasMol) the hot atoms are hidden by all regular atoms around the molten region. The middle image, where the transparency is medium, offers a clearer picture of the location of the hot atoms, while the one with highest transparency of the cold atoms allows a direct comparison with Fig. 9, where the vacancies are displayed. It can be seen that the region with large density of hot particles (Fig. 10) corresponds very well with the zone with high density of vacancies in the bulk (Fig. 9). Also, although there is a large number of vacancies near the surface, the number of hot particles near the surface is small, because their kinetic energy has already been dissipated at 3000 fs.

We note that at higher projectile energies the damage of the surface is more obvious, craters being formed as some atoms leave the target while others are relocated.

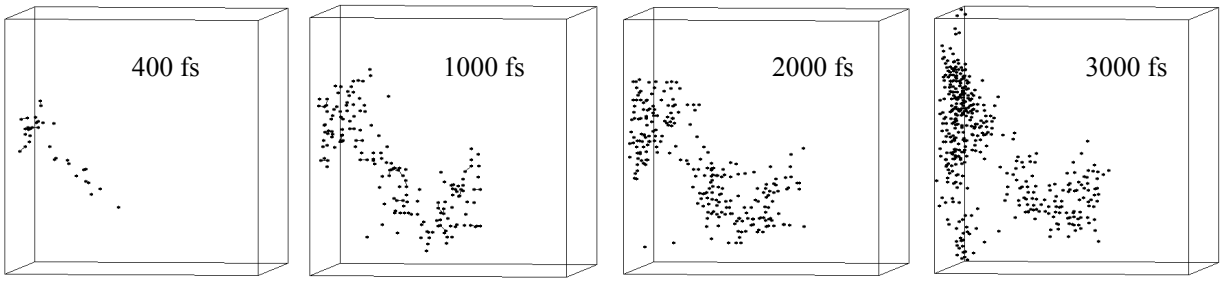

Fig. 9. Time evolution of all vacancies formed in a collision event in Pb, irradiated with a 1000 eV ion, displayed using RasMol. The vacancies are represented with dots.

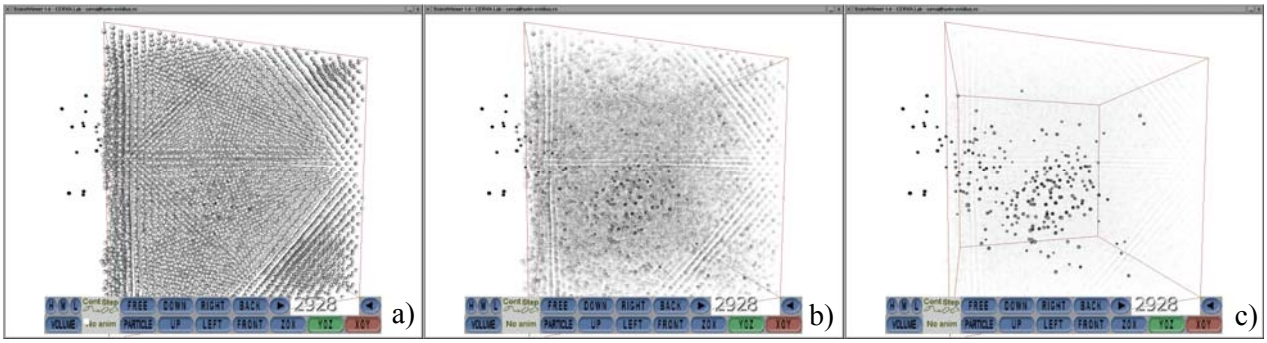

Fig. 10. Lateral view of a 37044 atom Pb target after 3000 fs from the impact with a 1000 eV ion, displayed using ScientView. The transparency of the Pb atoms depends on their kinetic energy, E_k, and was set to a) low (transparency equal to 0 for all particles, like in RasMol), b) medium (transparency 0 for particles with $E_k < 0.2$ eV and $1-E_k/200$ for the rest) and c) high (transparency 0 for particles with $E_k < 0.16$ eV and equal to $1-E_k/2000$ for the rest). The grey scale is identical to the one used in RasMol (see inset of Fig. 1).

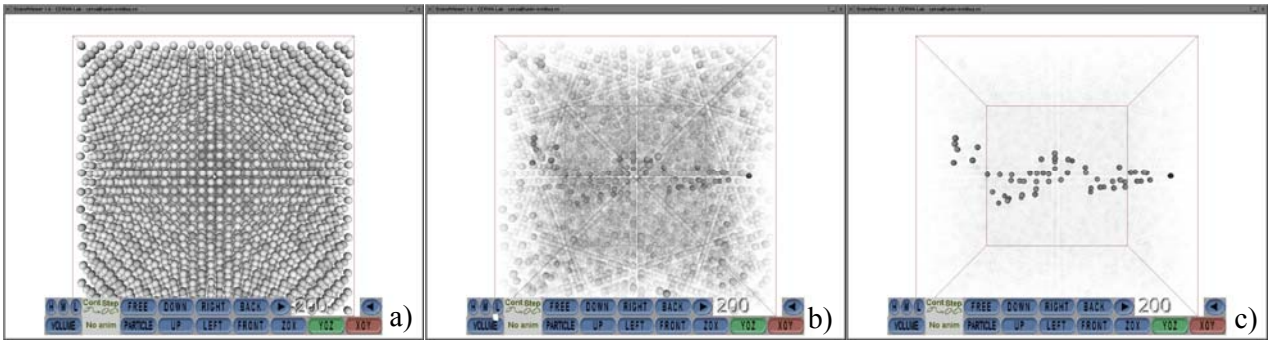

Fig. 11. Lateral view of the shock wave following a typical collision cascade in a 13500 atom Al target irradiated with a 500 eV particle, displayed using ScientView. The transparency of the Al atoms was set to: a) low (transparency equal to 0 for all particles, like in RasMol), b) medium (transparency 0 for particles with $E_k < 0.2$ eV and $1-E_k/200$ for the rest) and c) high (transparency 0 for particles with $E_k < 0.16$ eV and equal to $1-E_k/2000$ for the rest). The grey scale is identical to the one used in RasMol (see inset of Fig. 1).

Moving now to the last material, Al, a clear difference is noteworthy upfront. The 500 eV simulations for the 13500 atom Al target lead to complete penetration of the system, as presented in Fig. 11. Again, the images displayed using ScientView, using various transparencies of the target atoms, clearly show the shock wave left behind by the projectile, which passes through the target, leaving it on the right. The large range of the projectile in Al, prompted us in choosing for the same number of target atoms a lower projectile energy of 100 eV.

The time evolution of the total number of vacancies determined by a 100 eV ion impinging on a 13500 atom Al target is displayed in Fig. 12. The recrystallization process is slow in Al, 3000 fs being insufficient for the relaxation, although the peak in the number of vacancies is reached much earlier,

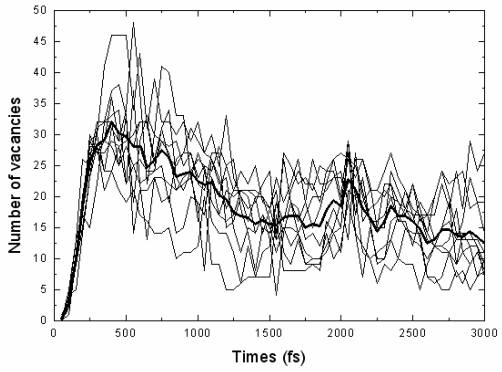

Fig. 12. Time evolution of the total number of vacancies generated in Al irradiated with a 100 eV ion. Ten individual events (with randomly selected initial recoil direction) and the average (thick line) are shown.

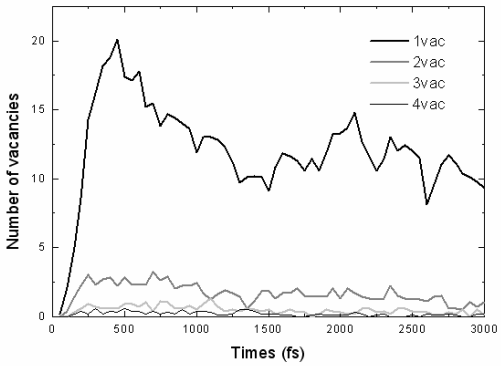

Fig. 13. Time evolution of the number of vacancies of mono-, di-, tri- and tetra-vacancies generated in an Al target by a 100 eV ion. The lines are averages calculated over 10 collision events.

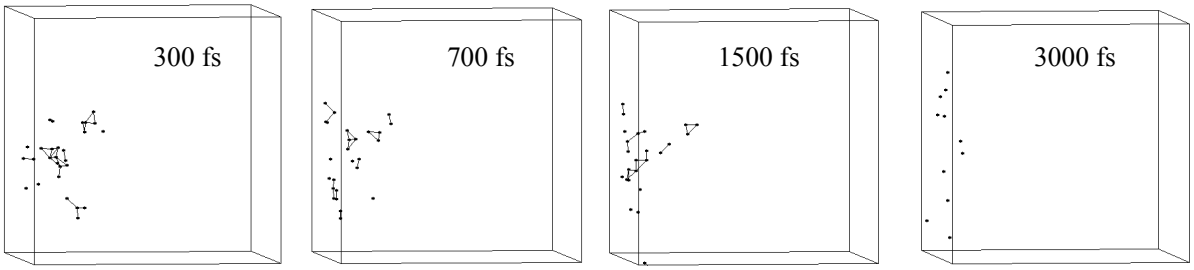

Fig. 14. Time evolution of all vacancies formed in a collision event in Al, irradiated with a 100 eV ion, displayed using RasMol. The vacancies are represented with dots while the vacancy clusters are connected with lines.

before 500 fs. Similar conclusions can be drawn from Fig. 13, which presents the average numbers of multiple vacancies. A more complete picture can be obtained when corroborating the results of Figs. 12 and 13 with the images in Fig. 14. We observe that the recrystallization in the bulk takes place much faster, the vacancies left after 3000 fs being mostly located near the surface.

A comparison between Cu, Ni, and Pb, is presented in Fig. 15, where the total number of vacancies averaged over ten 500 eV collision events is displayed as a function of time. We note that for Ni the maximum number of defects is almost three times smaller than for Cu, although they are both medium weight metals. Also, the recrystallization is much faster in Ni than in Cu, the number of defects decreasing to the expected value after less then 1000 fs.

Unlike the medium weight metals, Pb does not show a clear decrease of the number of vacancies before 3000 fs; a much longer simulation time is needed to observe the decrease. Although for Pb the number of defects is intermediate between the values for Ni and Cu, the regeneration of the crystal is very slow, as the atoms take a long time to take regular positions in the lattice.

It is worth analyzing the results of the molecular dynamics simulations in correlation with the values of the parameters defining the interparticle potential (see Table 1) and the physical properties of the materials studied (see Table 2). One observation is that Ni has the deepest potential, the highest melting temperature and the lowest number of vacancies generated by the 500 eV ion. This result is not surprising, as the depth of the potential is correlated with the dissociation energy. The higher the

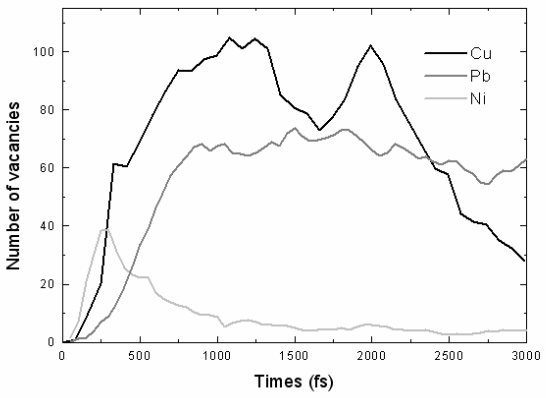

Fig. 15. Time evolution of the total number of vacancies produced in Cu, Ni and Pb by a 500 eV ion. The lines are averages calculated over 10 collision events.

Table 2. Values of the atomic number, atomic mass, melting temperature, density, ionic radius and lattice constant for the fcc metals studied.

Metal	Z	M (amu)	T_m (K)	ρ (kg/m^3)	r_i (Å)	a (Å)
Al	13	26.98	933.5	2700	1.25	4.05
Ni	28	58.71	1728.0	8908	1.35	3.52
Cu	29	63.55	1357.8	8920	1.35	3.61
Pb	82	207.2	600.6	11340	1.80	4.95

dissociation energy, the harder it is to melt the system and to generate Frankel defects.

The depth of the potential well is not the only factor influencing the number of vacancies created during the collision cascade. Aluminum has a deeper potential well than lead, but the number of defects is higher and, moreover, the 13500 atom target is easily penetrated at 500 eV impact. The large distance between the Al atoms (the atomic radius, r_i, is much less than half the equilibrium distance, r_e) is clearly correlated with the low density and justifies the long path of the projectile through the target. Lead is much better packed (it also has a much larger density) and, therefore, the path in the target is much shorter, leading to substantial damage near the surface (see Fig. 7).

The higher number of Frankel defects in Cu than in Ni can be correlated with both the smaller depth of the potential and the larger lattice constant. However, the larger number of vacancies in Cu than in Pb suggests that the dissociation energy alone cannot be the only factor influencing the number of defects. Likely, the high density of the heavy metal also plays a crucial role, causing a decrease of the number of defects.

The fastest recrystallization processes take place in Ni, the metal with the lowest width of the potential barrier (largest value of the α parameter of the interatomic potential). The recovery in Cu takes longer, the higher mass also playing a role; the heavier interstitial Cu atoms are slower in filling up the vacancies. Light and with small density, Al has a fast relaxation in the bulk but a slow recrystallization at the surface.

All metals studied have the same well packed fcc crystal structure and all recover very well in the bulk after the collision cascade. The defects left behind in the bulk after irradiation are the vacancies located near the core of the molten region and their corresponding interstitial atoms.

4. Conclusions

We studied, by means of MD simulations, the collision cascades and the time evolution of the complex vacancies produced by ion irradiation of metallic targets. We found that the number of vacancies increases abruptly in the collision phase and the thermal spike phase, reaches a maximum and decreases slowly afterwards. During the relaxation phase, the melted regions tend to recrystallize. The number of defects decreases, the vacancies migrating towards the surface and leaving behind only a small number.

The smallest number of defects and the fastest recrystallization was observed in the case of Ni. The largest path through the target and highest number of defects was seen for Al, while the slowest lattice regeneration was found for Pb. Except for Ni, we observed that even after 10 ps, the total number of vacancies was still much larger than the value expected based on the Kinchin-Pease equation. This result may be caused by the short duration of our simulation (much shorter than the ~1 ns required to also describe accurately the relaxation phase), but also by the large number of surface defects, not taken into account by the Kinchin-Pease model.

We examined the time evolution of complex vacancies (di-, tri- and tetra-vacancies) and we noticed that during the collision phase in the molten region clusters of multiple vacancies are formed while during the relaxation phase the clusters break into smaller clusters and mono-vacancies.

Although we used a simplified model of metallic materials, our results are consistent with some previous low temperature studies on similar types of fcc materials [1,18]. We expect that the use of more sophisticated potentials would improve on the values of the numbers of vacancies and of the recrystallization time affecting only moderately, however, the general trends we found.

Acknowledgements

This work was supported in part by the Romanian Ministry of Education and Research through the National University Research Council, grant CNCSIS A678/2006, and the National Authority for Scientific Research, grant CEEX-M3-C3-12350/2006. The authors are thankful to the research teams within the INTUITION project (FP6-IST-NMP-1-507248-2) and from CERV, Brest, France, as well as to the CERVA team from Ovidius University of Constanţa, Romania, for their constant support.

References

[1] K. Nordlund, M. Ghaly, R. S. Averback, M. Caturla, T. Diaz de la Rubia, J. Tarus Phys. Rev. B **57**, 7556 (1998).
[2] R. S. Averback, T. Diaz de la Rubia, in Solid State Physics **51** (eds F. Spaepen, et al.) 281–402 (Academic, New York, 1998).
[3] J. Tarus, K. Nordlund, Nucl. Instr. Meth. Phys. Res. B **212**, 281 (2003).
[4] K. Nordlund, J. Keinonen, M. Ghaly, R. S. Averback, Nature **49**, 398 (1999).
[5] M. Ghaly**,** K. Nordlund, R. S. Averback, Phil. Mag. A **79**, 795 (1999).
[6] C. C. Fu, J. D. Torre, F. Willaime, J. L. Bocquet and A. Barbu, Nature **68**, 4 (2005).
[7] C. Erginsoy, G. H. Vineyard, A. Englert, Phys. Rev. **133**, 595 (1964).

[8] M. P. Allen, D. J Tildesley, Computer simulation of liquids, Clarendon, Oxford, 1987.
[9] D. C. Rapaport, The art of molecular dynamics simulation, Cambridge University Press, Cambridge, 1995.
[10] P. M. Morse, Phys. Rev. **34**, 57 (1929).
[11] L. A. Girifalco, V. G. Weizer, Phys. Rev. **114**, 687 (1959).
[12] L. Verlet, Phys. Rev. **159**, 98 (1967); L. Verlet, Phys. Rev. **165**, 201 (1968).
[13] K. Nordlund, et al., The MDRANGE program, V1.0-V1.83b, Accelerator Laboratory, University of Helsinky, Finland, August 2002.
[14] K. Nordlund, J. Keinonen, A. Kuronen, Phys. Scripta **34,** 54 (1994).
[15] H. J. C. Berendsen, W. F. Van Gunsteren, A. Di Nola, J. R. Haak, J. Chem. Phys. **81,** 3684 (1984).
[16] G. H. Kinchin, R. S. Pease, Rep. Progr. Phys. **18**, 1 (1955).
[17] R. Schaeublin, M. J. Caturla, M. Wall, T. Felter, M. Fluss, B. D. Wirth, T. Diaz de la Rubia, M. Victoria, J. of Nuc. Mater. **307**, 988 (2002).
[18] K. Nordlund, R. S. Averback, Phys. Rev. B **56**, 2421 (1997).
[19] Herbert J. Bernstein, RasMol, version 2.7.3, Bellport, NY 11713-2803, USA, http://www.openrasmol.org/
[20] D. M. Popovici, ScientView, version 1.0, http://www.univ-ovidius.ro/cerva/scientview
[21] P. Reignier, F. Harrouet, S. Morvan, J. Tisseau, T. Duval, ARéVi: A Virtual Reality Multiagent Platform, in Proceedings VW'98, Paris, July 1-3, 1998, Springer Verlag, LNAI 1434, (1998) pp. 229-240.
[22] P. Reignier et al., ARéVi API software, the European Virtual Reality Center, CERV, Brest, France. http://www.cerv.fr/fr/activites/AReVi.php

*Corresponding author: girtu@univ-ovidius.ro